Molecular dynamics simulation of solar salt (NaNO3-KNO3) mixtures

Anagnostopoulos, Argyrios; Alexiadis, Alessio; Ding, Yulong

DOI:
10.1016/j.solmat.2019.04.019

Document Version
Peer reviewed version

Citation for published version (Harvard):
Anagnostopoulos, A, Alexiadis, A & Ding, Y 2019, 'Molecular dynamics simulation of solar salt (NaNO3-KNO3) mixtures', *Solar Energy Materials and Solar Cells*, vol. 200, 109897, pp. 1-9.
https://doi.org/10.1016/j.solmat.2019.04.019

Molecular Dynamics Simulation of Solar Salt ($NaNO_3$-KNO_3) mixtures

A. Anagnostopoulos, A. Alexiadis, Y. Ding

University of Birmingham, School of Chemical Engineering, Birmingham, United Kingdom

Corresponding Author: *axa1217@student.bham.ac.uk*

Center for Thermal Energy Storage, Birmingham, W. Midlands, United Kingdom

Keywords: Molecular, Simulation, Thermal, Energy Storage, Molten, Solar Salt, $NaNO_3$, KNO_3, Lennard-Jones

Abstract

Molten salts have extended applications in concentrated solar power (CSP) installations, both as heat transfer and energy storage materials. In this study, a set of Lennard-Jones interatomic parameters are introduced for simulating $NaNO_3$ and KNO_3, as well as their most frequently industrially used mixture the so-called solar-salt (60% $NaNO_3$ – 40% KNO_3). Local structures are studied via radial distribution functions. Furthermore, density, thermal conductivity, self-diffusivity, viscosity and surface tension are calculated, from the melting to decomposition temperature, and compared with experimental data. The local structures are calculated with both existing and presented interatomic potentials and are found to be in excellent agreement. Additionally, density, viscosity and surface tension present minor differences from literature data. Thermal conductivity, in terms of absolute values is in the proximity of reported data but is questionable in terms of trend. Finally, self-diffusion coefficients declinate from measured values, but are similar in terms of trend. The results are generally found to be in good agreement. This work represents the first validated effort in modelling molten nitrate salts mixtures at elevated temperatures using a Lennard-Jones potential, providing new tools that can aid in the fundamental understanding of molten salt structures at the molecular scale.

1 Introduction

Nowadays, 22.1% of global electricity production comes from renewable sources, with 1% of that being harvested from solar photovoltaics (PV) and concentrated solar power (CSP) installations. Hydro power is still the most common renewable technology. However, the use of solar PV and CSP grows at a rate of 30% every year [1].

Due to their low cost, good thermal properties and low vapor pressure molten salts have extended applications in CSP plants both as a heat transfer fluid and an energy storage medium. Molten nitrates are the most frequently used salts due to their thermal stability and relatively low cost. Their mixtures and specifically that of sodium and potassium nitrate, have a lower melting point than the independent components and thus a larger liquid phase range, leading to a larger operating range and minimal energy demand to remain in liquid form [2]. The optimal mixture is the pure molten salt eutectic (50% $NaNO_3$ – 50% KNO_3), but due to the higher cost, mixtures with 60% $NaNO_3$ and 40% KNO_3 are preferred; the properties of the later mixture are almost identical to the pure.

Study of the behavior of molten salts can further improve the understanding of their behavior, as well as identify areas where technical improvements are possible. Since high working temperatures make measurement of the material properties difficult, molecular dynamic (MD) simulations present an alternative for predicting these properties.

MD simulations of molten salts is an ongoing issue, starting in the late 1970s. The first works aimed to validate interatomic parameters of molten chlorides, due to their nuclear applications. Studies were conducted on the structure of molten sodium, potassium and lithium and rubidium chloride [3, 4, 5]. Studies on chloride have been on-going until today. Recently, Ding et al., studied the structure of NaCl and KCL and their mixtures and accurately calculated their properties using RNEMD methods [6]. In a similar work, Bengtson et al. investigated LiCl- KCL mixtures focusing on the changes in local structures and topological distributions [7]. Wang et al, computed the transport properties of LiF-BeF-ThF4 molten salt, using a polarizable force field, and observed that the electrical conductivity increases rapidly from 873K to 1273K, while the opposite was observed in the case of the viscosity [8,9]. Sun et al., also performed a study on 4 binary chloride systems (LiCl-RbCl, LiCl-CsCl, NaCl-RbCl and NaCl-CsCl). The study examined the impact of LiCL and NaCl on both the structures and the transport properties of Rbcl and CsCl. It was observed that the positive ions lead to weaker interactions between the counterions and hence affect the final structure of the mixture [10]. In terms of molten carbonates in another study by Ding et al., a series of calculations regarding local structures and transport properties were performed for binary carbonate mixtures of Na_2CO_3 and K_2CO_3 and in a subsequent publication the effect of the molar compositions on the local structures of the molten carbonate eutectics was further investigated [11,12]. The first MD work on nitrates mixture, to the best of our knowledge, was conducted by Adya et al. [13]. Mixtures of $NaNO_3$ and $NaNO_2$, including their eutectic, were examined by means of MD simulations. This study highlights the excellent agreement between the MD calculation and x-ray diffraction measurements. A more recent study on the specific heat capacity and thermal conductivity of molten $NaNO_3$, including the effect of SiO_2 nanoparticles, was conducted by Qiao et al. [14,15]. This study attributes the enhancement of the specific heat capacity to structural changes in the liquid-particle interface, caused by the nanoparticles. Jayaraman et al [16], calculated the liquid and crystal phases of $NaNO_3$, $LiNO_3$ and KNO_3 as well as their viscosities, thermal conductivities and specific heat capacities at 773K. Excellent agreement with experimental values was found for all properties investigated. In a subsequent study [17], the free energy and melting point of the mixtures of the three nitrates, in various concentrations, was also investigated. The behavior of Solar Salt with various concentrations of Al_2O_3 nanoparticles was investigated by Yanwei et al [18]. A set of ‘ad hoc’ Lennard-Jones parameters was proposed with the purpose of investigating the interaction energy of the nanoparticle on the base fluid. The study outlined the increase in coulombic forces in the presence of nanoparticles, as well as its effect on the specific heat capacity. Ni et al, modified the potential of Jayaraman, by changing the intramolecular parameters (bond, angle and improper forces). With this adjustment on the original Buckingham potential, an improved local structure prediction and property calculation was achieved. Furthermore, a mixture of $NaNO_3$ and KNO_3 was also simulated and the viscosity, thermal conductivity and density were calculated, with good agreement [19].

The accuracy of MD calculations depends on the availability of validated interatomic potentials. In the literature, several Lennard-Jones potentials are available for $NaNO_3$ and KNO_3 in aqueous solutions. These parameters, however, are not designed for molten phases. Buckingham parameters for pure molten $NaNO_3$ and KNO_3 do exist but are not suitable for mixtures mainly because mixing rules, like the Lorentz-Berthelot rules for the Lennard-Jones potential, are not available for the Buckingham potential. There are, therefore, no available interatomic potentials for the simulation of the solar salt.

This study proposes a set of Lennard-Jones parameters for molten $NaNO_3$-KNO_3 mixtures commonly used in industry (60% $NaNO_3$ – 40% KNO_3). To validate the proposed potential, local structural properties such as the radial distribution function (RDF) and transport properties such as viscosity, thermal conductivity and self-diffusivity as well as other properties such as density and surface tension are calculated and compared with experimental data available in the literature.

2 Theoretical Background

2.1 Interatomic Potential

The Lennard-Jones potential is used to describe pairwise interactions between atoms.

$$E_{LJ}(r) = 4\varepsilon[\left(\frac{\sigma}{r}\right)^{12} - \left(\frac{\sigma}{r}\right)^{6}] \quad (1)$$

where, σ is the finite distance at which the inter-particle potential is zero, $\underline{\varepsilon}$ the depth of the potential well and r the distance between two atoms

Columbic interactions are computed using

$$E_{Coulomb} = \frac{C\ q_i q_j}{er} \quad (2)$$

where, C is an energy-conversion constant, q_i the atom charge on atoms of type i, q_j the atom charge on atoms of type j, and e the dielectric constant.

The Lennard-Jones potential is relatively simple and computationally inexpensive (ideal for large atom systems). Moreover, for this potential, simple rules for calculating the cross-term interactions terms exist

$$\sigma_{ij} = \frac{\sigma_i + \sigma_i}{2} \quad (3)$$

$$\varepsilon_{ij} = \sqrt{\varepsilon_i \varepsilon_j} \quad (4)$$

The optimal values of ε and σ for the Lennard-jones potential for the pairs Na-Na, O-O, N-N and K-K are derived by fitting the $NaNO_3$ and KNO_3 Buckingham potentials of Jayaraman et al. [16]. The fitting was obtained by minimizing the least square error between the energy-distance curves of the two potentials. However, σ of the K-K pair was slightly modified from the initially obtained value in order to compensate for the under prediction of the density of KNO_3 at the melting point, by the Buckingham potential.

Cross-term interactions are calculated by means of the Lorentz-Berthelot mixing rules (Eq.3, Eq.4). Table 1 shows all the parameters used in the simulations.

Table 1. Lennard-Jones Parameters of $NaNO_3$ and KNO_3

Element	Q [e]	E [eV]	σ [Å]
Na	1	0.0066373	2.407
K	1	0.004336	3.188
N	0.95	0.004017509	3.431
O	-0.65	0.003469129	3.285

2.2 Intramolecular potential

The bond, angle and improper dihedral potentials of the nitrate (NO_3) structure are also accounted for. The N-O bond is simulated as a harmonic bond, with a harmonic bond constant of 525.0 (kcal·mol^{-1}·Å^{-1}) and an equilibrium bond length of 1.2676 (Å). The O-N-O angle is simulated as a harmonic angle with an angular constant of 105.0 (kcal·mol^{-1}·rad^{-2}) and an equilibrium angle of 120°. The improper O-N-O-O is simulated by a harmonic improper dihedral potential with constant 60.0 (kcal·mol^{-1}·rad^{-2}) and equilibrium angle of 0.0. The values for the intramolecular parameters are taken from the work of Qiao et al [14]. For all 3 cases the equation has the following format:

$$E = K(r - r_0)^2 \tag{5}$$

where, E is the harmonic potential, K a constant and r_0 the equilibrium bond length in the case of the bond, or the equilibrium angle in the case of the angle, or improper dihedral potential.

2.3 Simulation details

All simulations were performed using the LAMMPS software package [20]. Pure molten $NaNO_3$, KNO_3 and three mixtures (Table 2) were investigated. The mixture 59.66%-40.44% was selected due to it being the most commonly used mixture in the CSP industry; the 50%-50% molar is close to the pure eutectic mixture of the two salts, while the 3rd mixture (40.44-59.66%) is chosen to test the accuracy of the proposed potential when KNO_3 is the major component of the mixture.

Table 2. $NaNO_3$-KNO_3 Simulated Systems

$NaNO_3$-KNO_3 (%)	Sodium Ions	Potassium Ions	Total Atoms
59.66%-40.44%	960	384	6720
50%-50%	980	576	7780
40.44%-59.66%	860	508	6829

For the pure salts, the crystalline structures of $NaNO_3$ and KNO_3 are taken from Gonschorek et al and Adiwidjaja et al. respectively, and replicated in all dimensions, so that the resulting system consists of 4900 atoms [21,22]

Quenching is applied to the initial cell for equilibration. After a Polak-Ribiere structure minimization [23], the system is rapidly heated up from 293 to 1300K in 0.3 ns, in the NVT ensemble with a Nose-Hover thermostat and barostat [24]. Subsequently, it is equilibrated at 1300K for 0.5 ns in the NVT ensemble followed by a slow cool down up to the melting point in the NPT ensemble for 1 ns [25]. The final structure is obtained by further relaxing the system in the NVT ensemble for 0.5ns.

The cutoff of the interatomic potential is set at $15\dot{A}$, with long-term and columbic interactions being computed using Hockney's Particle-Particle Particle-Mesh (PPPM) method [26]. The equations of motions are solved using the Verlet leap-frog algorithm [27]. In all the simulations, the timestep is 0.001ps.

For the solar salt, the previous $NaNO_3$ and KNO_3 unit cells are replicated in a way to achieve the desired atom molar ratio. To avoid atom, overlap a variable random displacement of all atoms is applied in all 3 dimensions, using a specific routine in LAMMPS called fix move. Then a minimization and quenching process as described above is applied to obtain the final structure.

2.3 Calculated Properties

In this work, local structures (i.e. RDF), transport properties (i.e. viscosity, thermal conductivity) and surface tension for the pure molten salts, as well as their mixtures are calculated. The computational methodology for the calculation of each property is described hereafter.

2.3.1 Radial Distribution Function

The radial distribution function $g_{AB}(r)$, or pair correlation function, is the probability of encountering an atom B at a distance r from atom A. It is described by the following equation:

$$g_{AB}(r) = \frac{V n_B}{N_B 4pr^2 \mathrm{dr}} \tag{5}$$

where, V is the volume of the system, n_B the number of B particles in a spherical area of radius r with the center being atom A and N_B the total number of B particles.

2.3.2 Density

Density is calculated by means of

$$\rho = \frac{\sum_i N_i M_i}{N_A V_{NPT}} \quad (6)$$

Where N_i is the number of particles of type *i*, M_i the molar mass of type *i* particle, N_A Avogadro's constant and V_{NPT} the volume in the NPT ensemble.

2.3.3 Thermal Conductivity

The thermal conductivity is calculated as the time integral of the heat auto-correlation function *J* in a given direction by means of

$$k = \frac{1}{3Vk_BT}\int_0^\infty < J(0)J(t) > dt \quad (7)$$

where V is the volume, k_B the Boltzmann constant, *T* the temperature and <…> the ensemble averaging. J is the vector denoting the heat flux and is defined as

$$J = \mathrm{d}\sum_{\mathrm{i}} e_i v_i + \sum_{\mathrm{i}}\sum_{\mathrm{j}\neq\mathrm{i}} (F_{ij} v_i) r_{ij} \quad (8)$$

where e_i is the total energy, v_i the velocity of particle *i*, and F_{ij} the force on atom *i* exerted by neighbor atom *j*.

For the calculation of the thermal conductivity, the system is first equilibrated for 1 ns in the NVT ensemble using a Nose-Hoover thermostat at the desired temperature. After equilibration, heat flux vector values are averaged for 20 ns in the NVE ensemble in order to calculate the thermal conductivity at the desired temperature.

2.3.4 Viscosity

Shear viscosity is calculated similarly to the thermal conductivity:

$$\eta = \frac{V}{k_BT}\int_0^\infty < P_{xy}(0)\, P_{xy}(t) > \mathrm{dt} \quad (9)$$

where, *V* is the volume of the system, k_B the Boltzmann constant, *T* the temperature, and P_{xy} are the off- diagonal components of the stress tensor.

For the calculation of the viscosity, the system is first equilibrated for 10 ns in the NVE ensemble in the presence of a Langevin barostat. After equilibration, the barostat is turned off and stress tensor values are averaged for 1 ns in order to calculate the shear viscosity.

2.3.5 Surface Tension

Surface tension is calculated using the center of mass definition. The *z* dimension of the equilibrated simulation box is doubled, to avoid issues related to periodicity. Then the system is equilibrated in the NVT for 2 ns followed by a sampling for 10 ns in the NVE ensemble during which the pressure tensor data is averaged calculated. The surface tension is obtained by

$$\gamma = \frac{1}{2} L_z < P_{zz} - \frac{1}{2}\left(P_{xx} + P_{yy}\right) > \tag{10}$$

where, L_z is the total length of atoms in the z direction and $P_{xx,yy,zz}$ are the diagonal elements of the pressure tensor.

2.3.6 Diffusion Coefficient

Diffusion coefficient in MD simulations is calculated using the Einstein method, by means of the mean-squared displacement (MSD)

$$D = \frac{1}{6N} \cdot \lim_{t \to \infty} \frac{d}{dt} \sum_{i=1}^{N} < [\, \vec{r_i}(t) - \vec{r_i}(0)\,]^2 > \tag{11}$$

where, $[\, \vec{r_i}(t) - \vec{r_i}(0)\,]^2$ is the mean-square displacement of the selected group. The symbol $< >$ means that the property is averaged over the time of the simulation.

The system is equilibrated in the NVE ensemble, in the presence of a Langevin barostat for 1ns. After equilibration, the barostat is removed and the MSD values are averaged for 40 ns in the NVE ensemble. The MSD was plotted versus the time and the slope of the curve gave the value of the coefficient.

3. Results and Discussion

3.1 Radial Distribution Function

To validate the Lennard-Jones parameters proposed in this study, pure $NaNO_3$ and KNO_3 salts were simulated with both the Buckingham parameters from Jayaraman et al. [16], and the proposed Lennard-Jones potential.

In the case of the nitrogen and oxygen the distributions are almost identical, which is to be expected as bond, angle and improper forces are present and hold the nitrate structure firm. In the case of the sodium and potassium minor deviations can be seen between the two potentials, especially at the point of the first peak. This is to be expected and is related to the difference in mathematical formulations, between the Buckingham and the Lennard-Jones potentials. Furthermore, The K-K interaction potential, as explained in section 2.1, has been slightly modified to improve the accuracy of the density.

Na-Na

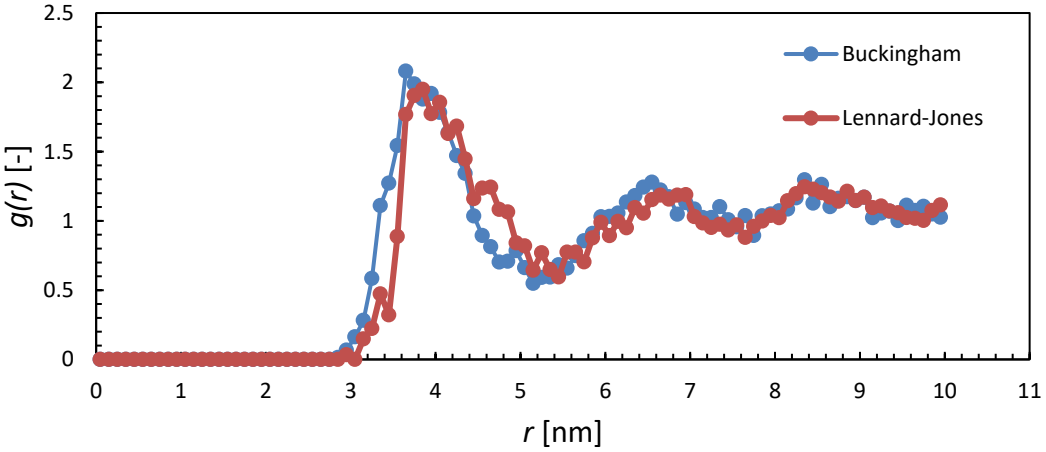
2.5
2
1.5
1
0.5
0
g(r) [-]
0
1
2
3
4
5
6
7
8
9
10
11
r [nm]
Buckingham
Lennard-Jones

K-K

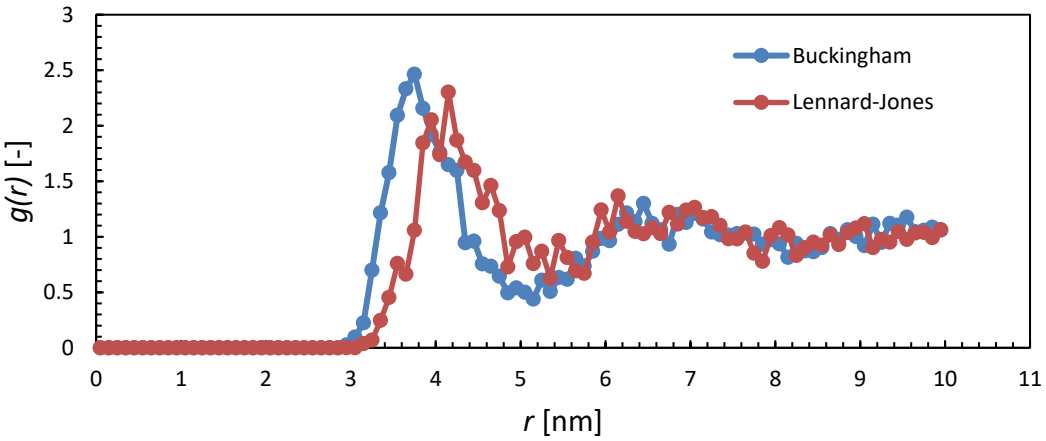
3
2.5
2
1.5
1
0.5
0
g(r) [-]
0
1
2
3
4
5
6
7
8
9
10
11
r [nm]
Buckingham
Lennard-Jones

N-N

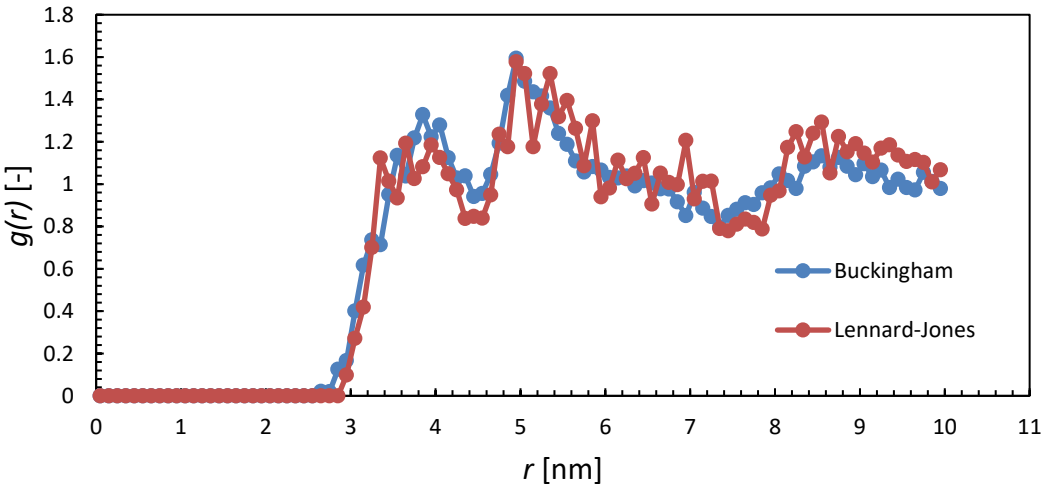
1.8
1.6
1.4
1.2
1
0.8
0.6
0.4
0.2
0
g(r) [-]
0
1
2
3
4
5
6
7
8
9
10
11
r [nm]
Buckingham
Lennard-Jones

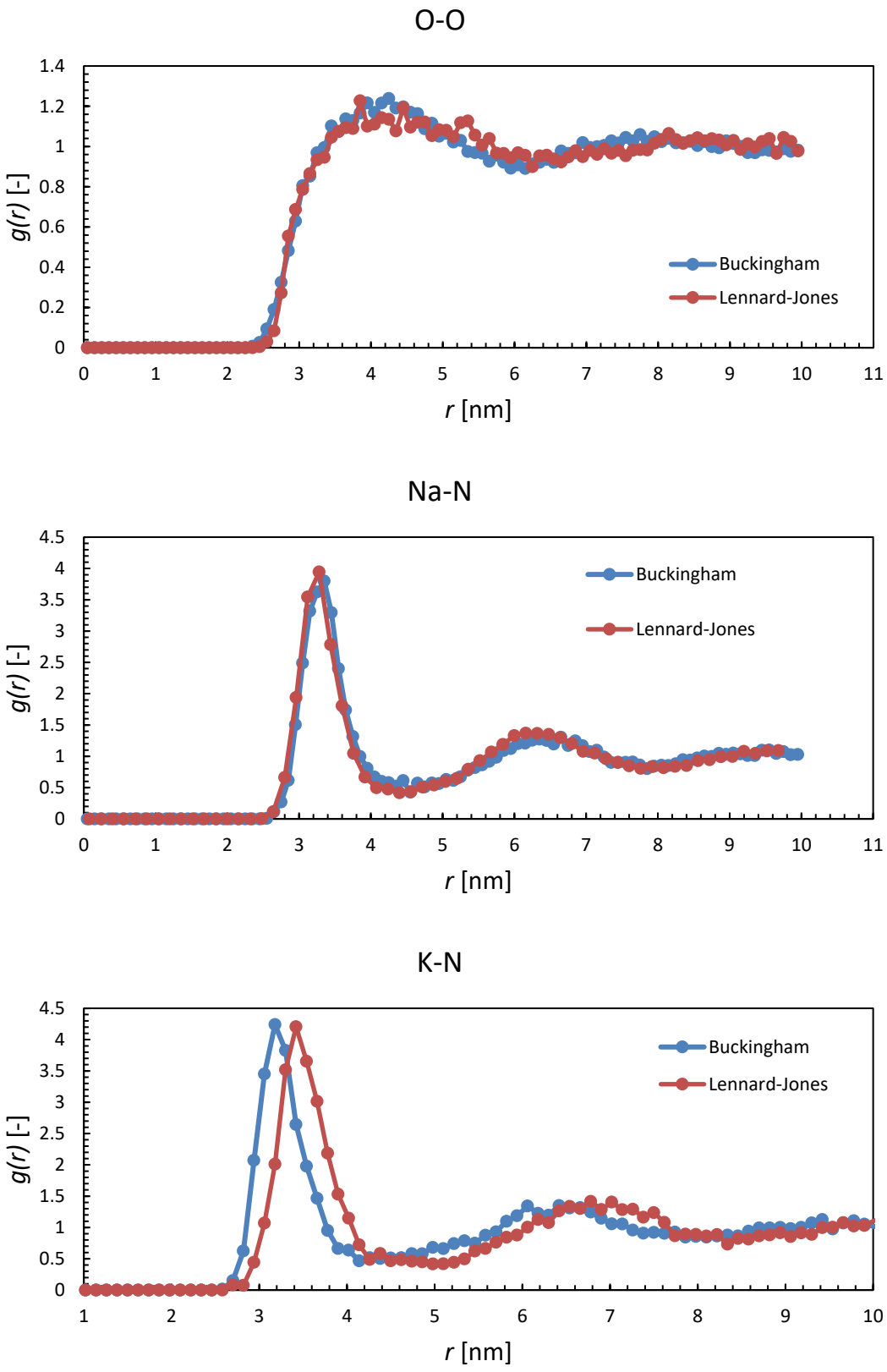

Figure 1. Radial Distribution function of $NaNO_3$ and KNO_3, comparison between Buckingham and Lennard-Jones potentials.

3.2 Transport Properties and Surface Tension for all simulated materials

In this work, the Lennard-Jones potential is used to calculate several properties (i.e. viscosity, thermal conductivity, surface tension) of the $NaNO_3$, the KNO_3 and their mixtures with different compositions. Results are compared against available experimental data. Results are gathered in Table 3. The calculated properties were compared across a range of temperatures that comprises the entire liquid phase, between the melting and the decomposition point, for each mixture. The melting temperatures are considered to be 310 and 335 °C for $NaNO_3$ and KNO_3, 250 °C for the 60%-40% and 40%- 60% and 220 °C for the 50%-50% mixture. Decomposition temperatures vary depending on the heating rate and atmospheric conditions. The lowest temperatures under which no decomposition occurs under any conditions are at 400 °C for $NaNO_3$ and KNO_3, with the case of the KNO_3 representing a boiling point. In the case of the mixtures it is assumed that decomposition starts at 450 °C.

For the individual components the density prediction is excellent. In terms of the mixtures, slight variations in density are attributed to the empirical nature of the cross-term interactions. Viscosity appears to be overestimated in the case of the individual components, while it is underestimated in the case of the mixtures. In all cases absolute values are within 12.32% deviation from experimental measurements. Thermal conductivity in all cases is overpredicted and presents an increasing trend. This, as further discussed in section 3.2.2, is linked to both the uncertainty of the thermal conductivity and also the way that the property is defined in the molecular level. Diffusion coefficients are highly underappreciated in all cases. However, from the calculated results, the advantage of MD studies can be recognized. Values are obtained in cases where experimental measurements are lacking, providing, if not a perfect prediction, an accurate estimation of the desired properties. Surface tension values are overappreciated in all cases, but differences from experimental measurements are in no case higher than 14.56%. In general, the calculated properties provided with the use of the presented interatomic parameters are in good agreement with literature data.

Table 3. Comparison between experimental measurements and calculated values for $NaNO_3$, KNO_3 and their mixtures for various properties [28–32].

Material		$NaNO_3$		KNO_3		60% $NaNO_3$-40% KNO_3		50% $NaNO_3$-50% KNO_3		40%$NaNO$-60% KNO_3	
Temperature		T_{melt}	T_{dec}	T_{melt}	T_{dec}	T_{melt}	T_{dec}	T_{melt}	T_{dec}	T_{melt}	T_{dec}
Density ρ (g/cm^3)	Exp	1.93	1.85	1.86	1.79	1.98	1.79	1.93	1.80	1.93	1.81
	Sim	1.93	1.86	1.86	1.80	2.05	1.86	2.02	1.91	2.08	1.94
Viscosity η (mP/s)	Exp	2.94	2.17	2.57	2.07	4.61	1.48	4.72	1.57	-	-
	Sim	3.42	2.47	2.27	1.92	3.87	1.51	3.91	1.79	3.46	1.63
Thermal Conductivity k (W/m·K)	Exp	0.51	0.50	0.41	0.38	0.48	0.53	0.48	0.53	0.46	0.51
	Sim	0.64	0.68	0.58	0.54	0.56	0.44	0.59	0.54	0.71	0.62
Self-Diffusion D ($cm^2/s \cdot 10^{-5}$)	Exp	3.37	4.93	1.48	2.22	1.36	3.23	-	-	-	-
	Sim	0.893	1.76	0.364	0.823	0.352	1.532	0.124	1.345	0.257	1.834
Surface Tension γ (mN/m)	Exp	119.8	115.5	116.7	107.3	118.9	108.2	120.7	107.1	120.1	106.3
	Sim	135.7	129.4	128.6	122.2	136.3	114.2	133.4	115.2	136.5	119.8

In the next sections, we focus on the eutectic mixture (60% $NaNO_3$-40% KNO_3), which is by far the most frequently used molten salt in CSP industry.

3.2.1 Density

The density of the solar salt, throughout its entire liquid phase temperature range can be seen in Fig 2. The average difference between computed and measured values is 6.1%. This could be attributed to the cross-term interactions between Na and K, which are based on the mixing rule, that contains some degree of inaccuracy. Naturally at higher temperature levels, kinetic energy causes the molecular structure of the liquid to become more spread and hence the density is reduced.

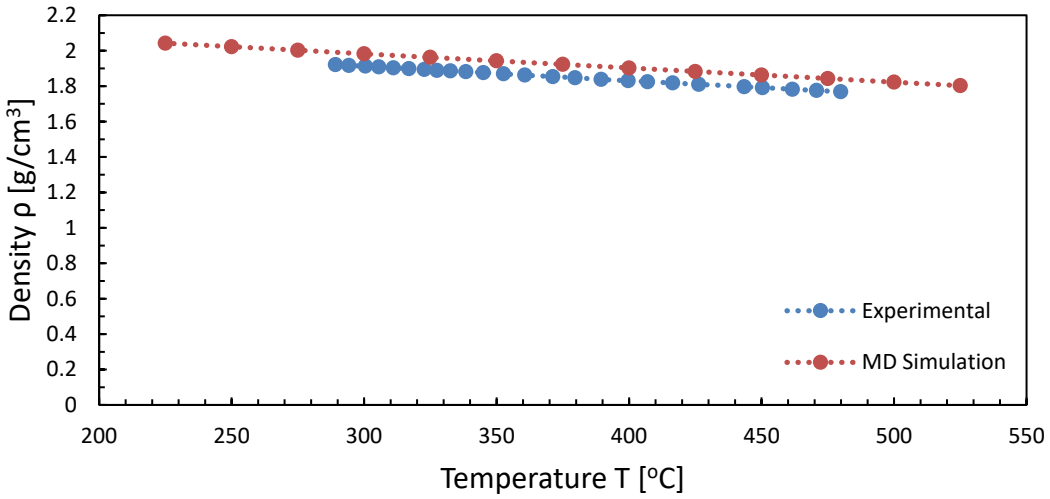

Figure 2. Density of Solar Salt (60% $NaNO_3$-40% KNO_3), comparison with experimental data [28].

3.2.2 Thermal Conductivity

Simulations overall agree with the available experimental data. However (Figure 2), the trend is not the same for T > 400 °C. We do not have a clear explanation for this difference, which also occurs in other MD studies concerning molten nitrate salts, using the Buckingham potential [19]. However, it must be noted that experimental thermal conductivity measurements are particularly difficult at these temperatures and often are not consistent with each other (Fig. 2).

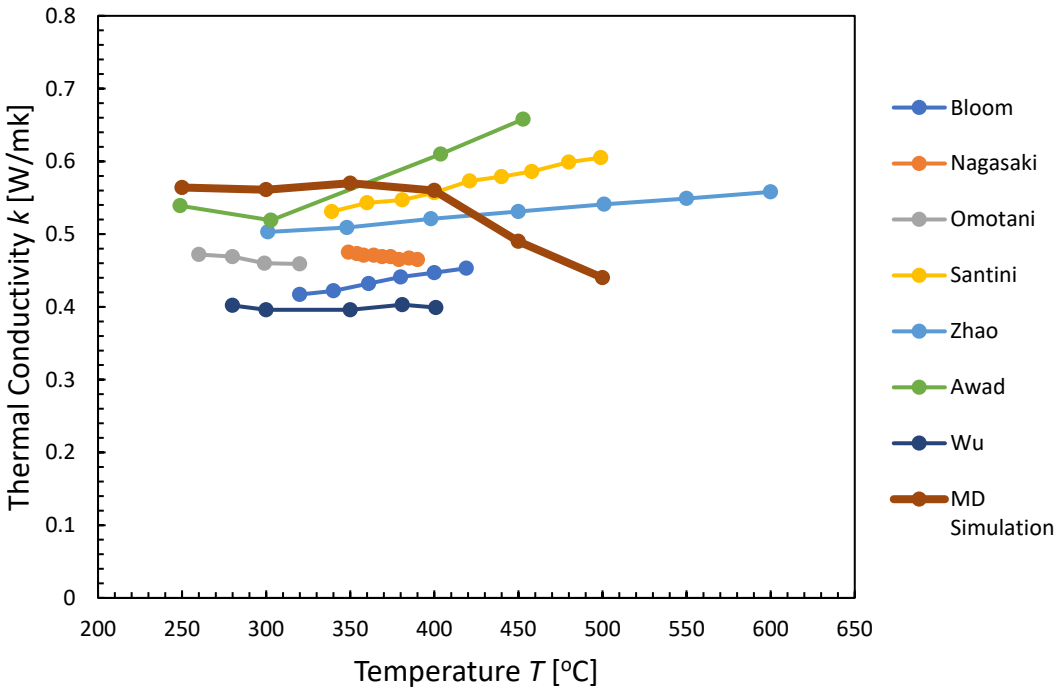

Figure 3. Thermal Conductivity of Solar Salt (60% $NaNO_3$-40% KNO_3), comparison with experimental data [2,32–36].

3.2.3 Viscosity

A comparison between the calculated and measured values is shown in Fig. 4: average difference is around 10%. The trend of the molten salt density with respect to temperature (Fig. 2), confirms that at higher temperatures, the molten liquid becomes less dense, with distances between the atoms becoming larger, leading to a smaller resistance to shear stress and thus an expected reduction in the viscosity.

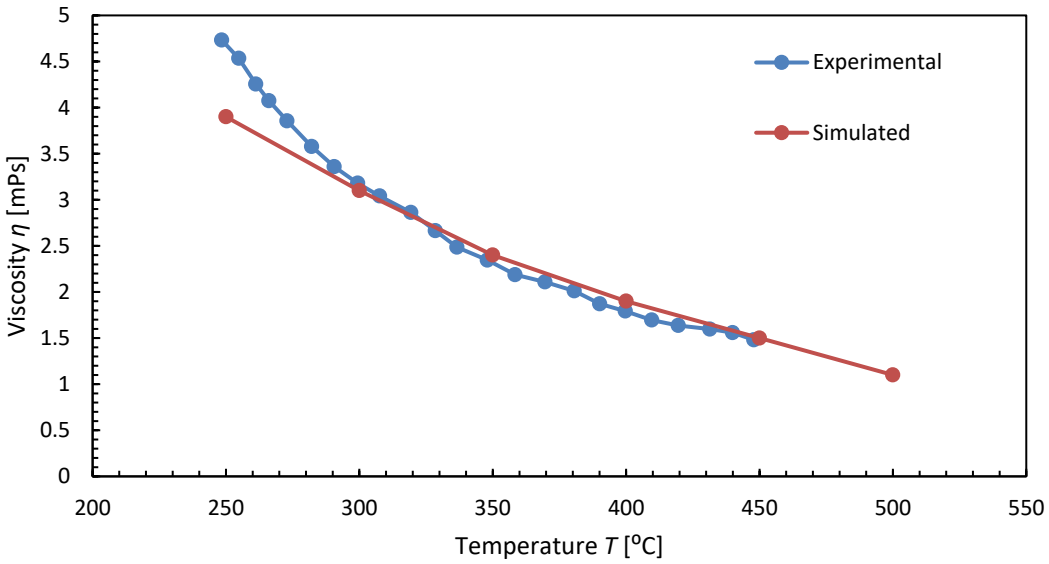

Figure 4. Viscosity of Solar Salt (60% $NaNO_3$-40% KNO_3), comparison with experimental data [28].

3.2.4 Surface Tension

Both experimental and calculated results follow the same trend (Fig. 5). No experimental data were found for values above 400 °C. Average percentage difference between experimental and simulated values is 8.6%.

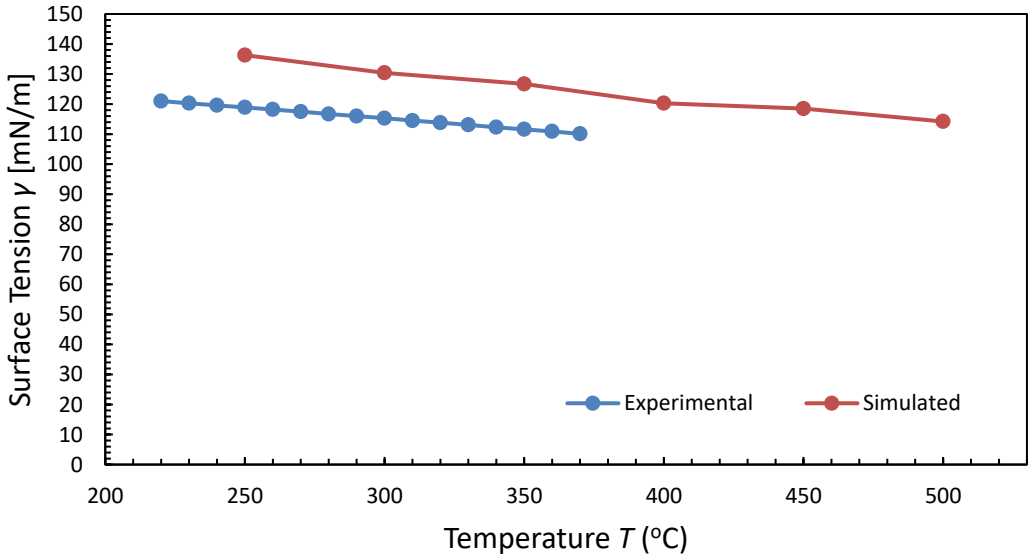

Figure 5. Surface Tension of Solar Salt (60% $NaNO_3$-40% KNO_3), comparison with experimental data [31]

3.2.5 Self-Diffusion Coefficient

In Figure 6 the self-diffusion coefficients of the solar salt are compared between experimental measurements and calculated values. Although the trends are similar, there is a more significant variation between measured and calculated values for the self-diffusivity than for other properties. In general, self-diffusivity is a property that is often not very accurate in MD simulations and the average error (94.25%) obtained here is comparable to other simulations [37–39].

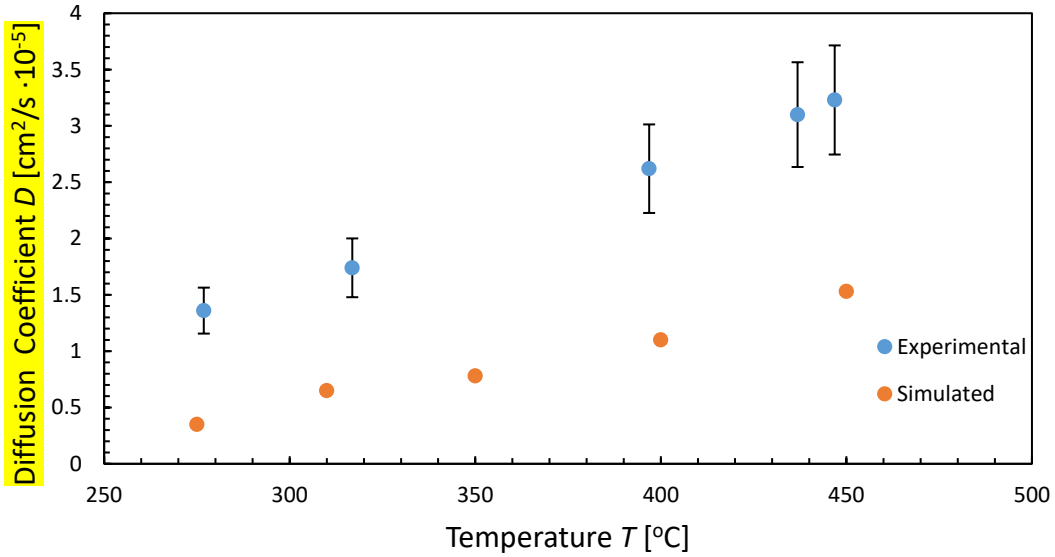

Figure 6. Diffusion Coefficient of Solar Salt (60% $NaNO_3$-40% KNO_3), comparison with experimental data [30].

Conclusions

In this study, an original set of Lennard-Jones parameters are presented capable of accurately representing the behavior of pure $NaNO_3$ and KNO_3 molten nitrate salts and their mixtures, throughout temperature range typical of solar applications.

For validation, the simulated local structures of pure $NaNO_3$ and KNO_3 are compared with those obtained in a previous study on the same materials using the Buckingham potential. The peaks of the RDFs are in good agreement in all cases, except for the case of the KNO_3 that has been slightly altered to match the density at the melting point.

Furthermore, the simulated transport properties (density, thermal conductivity, viscosity), as well as surface tension, of both pure molten $NaNO_3$ and KNO_3 are investigated. Density, viscosity and surface tension are in prefect agreement with literature data with a difference not higher, in any instance, than 17.11% from experimental data. Self-diffusivity shows divergence from the literature values but is similar in terms of trend. Thermal conductivity is in good agreement in terms of absolute values but shows a trend opposite to the majority of the literature data. Several factors affect the measurement and calculation of thermal

conductivity, which makes it very difficult to systematically obtain a similar value. Further research is required, both experimental and computational to investigate this phenomenon.

Atomic interactions are of high importance and effectively govern the behavior at the interface of materials. A set Lennard-Jones parameters, such as the one presented in this study for the molten salt mixtures. can provide essential contribution. This is due to validated existing techniques, for cross-term interatomic parameters computation, that the Lennard-Jones potential provides. Examples of such trending scenarios are in molten salt-nanoparticle systems, where the nanoparticle salt interface can be investigated and insight in property enchantment can be provided, composite material formulation, where information on the pores and capillary forces can be given and wetting/corrosion phenomena, where surface alteration can be visualized in the atomic level. Issues related to this type phenomena, in elevated temperatures, exist not only the solar industry, but also in nuclear power sector. MD simulations can provide a solution, in conditions, where performing experiments can be difficult, expensive and in cases of microstructure analysis, problematic. A simple and computationally inexpensive tool is provided in this work to provide answers to the aforementioned problems.

References

[1] N. Kannan, D. Vakeesan, Solar energy for future world: - A review, Renew. Sustain. Energy Rev. (2016). doi:10.1016/j.rser.2016.05.022.

[2] A. Awad, H. Navarro, Y. Ding, D. Wen, Thermal-physical properties of nanoparticle-seeded nitrate molten salts, Renew. Energy. (2018). doi:10.1016/j.renene.2017.12.026.

[3] F.G. Edwards, J.E. Enderby, R.A. Howe, D.I. Page, The structure of molten sodium chloride, J. Phys. C Solid State Phys. (1975). doi:10.1088/0022-3719/8/21/018.

[4] C. Caccamo, M. Dixon, Molten alkali-halide mixtures: A molecular-dynamics study of Li/KCl mixtures, J. Phys. C Solid State Phys. (1980). doi:10.1088/0022-3719/13/10/009.

[5] E.W.J. Mitchell, P.F.J. Poncet, R.J. Stewart, The ion pair distribution functions in molten rubidium chloride, Philos. Mag. (1976). doi:10.1080/14786437608222045.

[6] J. Ding, G. Pan, L. Du, J. Lu, X. Wei, J. Li, W. Wang, J. Yan, Theoretical prediction of the local structures and transport properties of binary alkali chloride salts for concentrating solar power, Nano Energy. (2017). doi:10.1016/j.nanoen.2017.07.020.

[7] A. Bengtson, H.O. Nam, S. Saha, R. Sakidja, D. Morgan, First-principles molecular dynamics modeling of the LiCl-KCl molten salt system, Comput. Mater. Sci. (2014). doi:10.1016/j.commatsci.2013.10.043.

[8] J. Wang, Z. Sun, G. Lu, J. Yu, Molecular dynamics simulations of the local structures and transport coefficients of molten alkali chlorides, J. Phys. Chem. B. (2014). doi:10.1021/jp5050332.

[9] J. Wang, J. Wu, Z. Sun, G. Lu, J. Yu, Molecular dynamics study of the transport properties and local structures of molten binary systems (Li, Na)Cl, (Li, K)Cl and (Na, K)Cl, J. Mol. Liq. (2015). doi:10.1016/j.molliq.2015.06.021.

[10] Z. Sun, L. Cai, H. Ni, G. Lu, X. Song, J. Yu, Investigation of the local structures and transport properties of quaternary molten alkali chloride systems by MD simulations for liquid metal batteries, J. Appl. Electrochem. (2018). doi:10.1007/s10800-018-1197-z.

[11] J. Ding, G. Pan, L. Du, J. Lu, W. Wang, X. Wei, J. Li, Molecular dynamics simulations of the local structures and transport properties of Na<inf>2</inf>CO<inf>3</inf> and K<inf>2</inf>CO<inf>3</inf>, Appl. Energy. (2017). doi:10.1016/j.apenergy.2017.07.019.

[12] J. Ding, G. Pan, L. Du, J. Lu, W. Wang, X. Wei, J. Li, Molecular dynamics simulations of the local structures and transport properties of Na2CO3 and K2CO3, Appl. Energy. (2018). doi:10.1016/j.apenergy.2017.07.019.

[13] A.K. Adya, R. Takagi, K. Kawamura, M. Mikami, Structural determination of molten NaNO3, NaNO2and their eutectic mixture by molecular dynamics simulation and X-ray diffraction, Mol. Phys. (1987). doi:10.1080/00268978700102161.

[14] G. Qiao, M. Lasfargues, A. Alexiadis, Y. Ding, Simulation and experimental study of the specific heat capacity of molten salt based nanofluids, Appl. Therm. Eng. (2017). doi:10.1016/j.applthermaleng.2016.07.159.

[15] G. Qiao, A. Alexiadis, Y. Ding, Simulation study of anomalous thermal properties of molten nitrate salt, Powder Technol. (2017). doi:10.1016/j.powtec.2016.11.019.

[16] S. Jayaraman, A.P. Thompson, O.A. Von Lilienfeld, E.J. Maginn, Molecular simulation of the thermal and transport properties of three alkali nitrate salts, Ind. Eng. Chem. Res. (2010). doi:10.1021/ie9007216.

[17] S. Jayaraman, A.P. Thompson, O.A. Von Lilienfeld, Molten salt eutectics from atomistic simulations, Phys. Rev. E - Stat. Nonlinear, Soft Matter Phys. (2011). doi:10.1103/PhysRevE.84.030201.

[18] Y. Hu, Y. He, Z. Zhang, D. Wen, Effect of Al2O3nanoparticle dispersion on the specific heat capacity of a eutectic binary nitrate salt for solar power applications, Energy Convers. Manag. (2017). doi:10.1016/j.enconman.2017.03.062.

[19] H. Ni, J. Wu, Z. Sun, G. Lu, J. Yu, Molecular simulation of the structure and physical properties of alkali nitrate salts for thermal energy storage, Renew. Energy. 136 (2019) 955–967. doi:10.1016/j.renene.2019.01.044.

[20] S. Plimpton, Fast parallel algorithms for short-range molecular dynamics, J. Comput. Phys. (1995). doi:10.1006/jcph.1995.1039.

[21] G. Gonschorek, H. Weitzel, G. Miehe, H. Fuess, W.W. Schmahl, The crystal structures of NaNO3 at 100 K, 120 K and 563 K, Zeitschrift Für Krist. - Cryst. Mater. 215 (2000). doi:10.1524/zkri.2000.215.12.752.

[22] G. Adiwidjaja, D. Pohl, Superstructure of α-phase potassium nitrate, Acta Crystallogr. Sect. C Cryst. Struct. Commun. 59 (2003) i139–i140. doi:10.1107/S0108270103025277.

[23] D. Sheppard, R. Terrell, G. Henkelman, Optimization methods for finding minimum energy paths, J. Chem. Phys. (2008). doi:10.1063/1.2841941.

[24] G.J. Martyna, D.J. Tobias, M.L. Klein, Constant pressure molecular dynamics algorithms, J. Chem. Phys. (1994). doi:10.1063/1.467468.

[25] M.E. Tuckerman, J. Alejandre, R. López-Rendón, A.L. Jochim, G.J. Martyna, A Liouville-operator derived measure-preserving integrator for molecular dynamics simulations in the isothermal-isobaric ensemble, J. Phys. A. Math. Gen. (2006). doi:10.1088/0305-4470/39/19/S18.

[26] J.V.L. Beckers, C.P. Lowe, S.W. De Leeuw, An iterative PPPM method for simulating

coulombic systems on distributed memory parallel computers, Mol. Simul. (1998). doi:10.1080/08927029808022044.

[27] W.F. Van Gunsteren, H.J.C. Berendsen, A Leap-Frog Algorithm for Stochastic Dynamics, Mol. Simul. (1988). doi:10.1080/08927028808080941.

[28] N. Pfleger, T. Bauer, C. Martin, M. Eck, A. Wörner, Thermal energy storage - overview and specific insight into nitrate salts for sensible and latent heat storage, Beilstein J. Nanotechnol. (2015). doi:10.3762/bjnano.6.154.

[29] G.J. Janz, Molten Salts Data as Reference Standards for Density, Surface Tension, Viscosity, and Electrical Conductance: KNO3and NaCl, J. Phys. Chem. Ref. Data. 9 (1980) 791–830. doi:10.1063/1.555634.

[30] G.J. Janz, N.P. Bansal, Molten Salts Data: Diffusion Coefficients in Single and Multi Component Salt Systems, J. Phys. Chem. Ref. Data. (1982). doi:10.1063/1.555665.

[31] G.J. Janz, U. Krebs, H.F. Siegenthaler, R.P.T. Tomkins, Molten Salts: Volume 3 Nitrates, Nitrites, and Mixtures: Electrical Conductance, Density, Viscosity, and Surface Tension Data, J. Phys. Chem. Ref. Data. (1972). doi:10.1063/1.3253103.

[32] Q.G. Zhao, C.X. Hu, S.J. Liu, H. Guo, Y.T. Wu, The thermal conductivity of molten NaNO3, KNO3, and their mixtures, in: Energy Procedia, 2017. doi:10.1016/j.egypro.2017.12.761.

[33] Y. Nagasaka, A. Nagashima, The thermal conductivity of molten NaNO3 and KNO3, Int. J. Thermophys. 12 (1991) 769–781. doi:10.1007/BF00502404.

[34] T. Omotani, Y. Nagasaka, A. Nagashima, Measurement of the thermal conductivity of KNO3-NaNO3 mixtures using a transient hot-wire method with a liquid metal in a capillary probe, Int. J. Thermophys. 3 (1982) 17–26. doi:10.1007/BF00503955.

[35] R. Santini, L. Tadrist, J. Pantaloni, P. Cerisier, Measurement of thermal conductivity of molten salts in the range 100–500°C, Int. J. Heat Mass Transf. 27 (1984) 623–626. doi:10.1016/0017-9310(84)90034-6.

[36] Y. Wu, J. Li, M. Wang, H. Wang, Y. Zhong, Y. Zhao, M. Wei, Y. Li, Solar salt doped by MWCNTs as a promising high thermal conductivity material for CSP, RSC Adv. (2018). doi:10.1039/c8ra03019g.

[37] G. Pranami, M.H. Lamm, Estimating Error in Diffusion Coefficients Derived from Molecular Dynamics Simulations, J. Chem. Theory Comput. (2015). doi:10.1021/acs.jctc.5b00574.

[38] G. Hummer, Position-dependent diffusion coefficients and free energies from Bayesian analysis of equilibrium and replica molecular dynamics simulations, New J. Phys. (2005). doi:10.1088/1367-2630/7/1/034.

[39] Y.C. Lin, X. Chen, Investigation of moisture diffusion in epoxy system: Experiments and molecular dynamics simulations, Chem. Phys. Lett. (2005). doi:10.1016/j.cplett.2005.07.022.

Table of Tables

Table of Figures